The Astronomical Journal, 134:1360–1367, 2007 October

μ-PhotoZ: PHOTOMETRIC REDSHIFTS BY INVERTING THE TOLMAN SURFACE BRIGHTNESS TEST

Michael J. Kurtz, Margaret J. Geller, Daniel G. Fabricant, and William F. Wyatt
Harvard-Smithsonian Center for Astrophysics, Cambridge, MA 02138, USA; kurtz@cfa.harvard.edu

and

Ian P. Dell'Antonio
Department of Physics and Astronomy, Brown University, Providence, RI 02912, USA
Received 2007 April 25; accepted 2007 July 3

ABSTRACT

Surface brightness is a fundamental observational parameter of galaxies. We show, for the first time in detail, how it can be used to obtain photometric redshifts for galaxies, the μ-PhotoZ method. We demonstrate that the Tolman surface brightness relation, $\mu \propto (1+z)^{-4}$, is a powerful tool for determining galaxy redshifts from photometric data. We develop a model using μ and a color percentile (ranking) measure to demonstrate the μ-PhotoZ method. We apply our method to a set of galaxies from the SHELS survey, and demonstrate that the photometric redshift accuracy achieved using the surface brightness method alone is comparable with the best color-based methods. We show that the μ-PhotoZ method is very effective in determining the redshift for red galaxies using only two photometric bands. We discuss the properties of the small, skewed, non-Gaussian component of the error distribution. We calibrate μ_r, $(r-i)$ from the SDSS to redshift and tabulate the result, providing a simple but accurate look-up table to estimate the redshift of distant red galaxies.

Key words: galaxies: distances and redshifts — galaxies: photometry — methods: data analysis — techniques: photometric

1. INTRODUCTION

Tolman (1930) and Hubble & Tolman (1935) first showed that in an expanding universe the surface brightness of a galaxy is a strong function of the redshift, SB $\propto (1+z)^{-4}$ or $\mu = \mu_0 + 10 \log (1+z)$. Hubble & Tolman (1935) suggested that this effect could be used as a distance indicator and as a test of various cosmological scenarios (the Tolman test).

Baum (1957) was the first to show that the shifting of spectral features as a function of redshift (in particular the 4000 Å break) causes color changes which can be calibrated to estimate a redshift. Interestingly, the discussion with Hoyle following Baum (1962) demonstrates an understanding that this effect might be combined with or be complementary to the surface brightness effect for redshift estimation. At the time of the discussion, the steady state hypothesis was still quite viable, and thus the exact nature of the surface brightness effect was not known. More recently, Sandage & Lubin (2001) and Pahre et al. (1996) measured the effect; various systematics, including galaxy luminosity evolution, prevent these measures from being definitive, but the true relation is very close to $(1+z)^{-4}$.

Typically photometric redshifts are derived from color differences as a function of total magnitude. Some techniques fit model spectra (e.g., Baum 1957; Budavári et al. 2001; Bolzonella et al. 2000), others directly calibrate the data set (e.g., Firth et al. 2003; Kodama et al. 1999; Feldmann et al. 2006), and still others combine these two methods into a hybrid (e.g., Padmanabhan et al. 2005, hereafter P05). Several proponents of the neural network method remark that surface-brightness-related measures could be added to their input parameters (e.g., Margoniner et al. 2005; Suchkov et al. 2005). By including the Petrosian 50% and 90% flux radii, Wadadekar (2005) found a 15% improvement in the mean redshift error.

Here we demonstrate that surface brightness provides a highly effective redshift estimator for the reddest galaxies in each surface brightness interval, yielding very accurate photometric redshifts from either *r*- and *i*-, or *r*- and *z*-band observations. We indicate how other color combinations might be used. We present the μ_r, $(r-i)$ calibration to redshift for red galaxies in the SDSS. One powerful advantage of this method is that only two bands are required for its application.

We present the data in § 2, and in § 3 we introduce the μ-PhotoZ technique and discuss its physical basis and limitations. We briefly indicate the extension of our technique to other bandpasses in § 4. The technique is applied in § 5, and we discuss the nature of the error distribution in detail. In § 6 we apply our method to the SDSS.

2. DATA

We combine data from three large surveys to create a set of measures suitable for demonstration of the μ-PhotoZ technique: (1) a magnitude-limited galaxy catalog from the Deep Lens Survey (DLS; Wittman et al. 2006), (2) redshifts and spectral types from the Smithsonian Hectospec Lensing Survey (SHELS; Geller et al. 2005), and (3) photometry and spectroscopy from the fourth and fifth data releases of the Sloan Digital Sky Survey (SDSS; Adelman-McCarthy et al. 2006).

2.1. *DLS*

SHELS used the DLS deep *R*-band photometry from the $2^\circ \times 2^\circ$ field F2 (9^h20^m, $+30^\circ00'$ [J2000.0]) to select galaxies for redshift measurements with Hectospec (Fabricant et al. 2005). We used the difference between magnitudes within the $1.5''$ and $5''$ apertures and the FWHM to a Gaussian fit as star/galaxy classifiers. It is possible to derive photometric redshifts based on *colors* from the deep multicolor DLS data (Margoniner & Wittman 2007).

The extended (scattering) halos around bright stars significantly contaminate the brightness measures of faint galaxies. We have excluded all objects within a magnitude-determined radius of every bright star; about 5% of the total area of the survey is thus removed from further consideration.

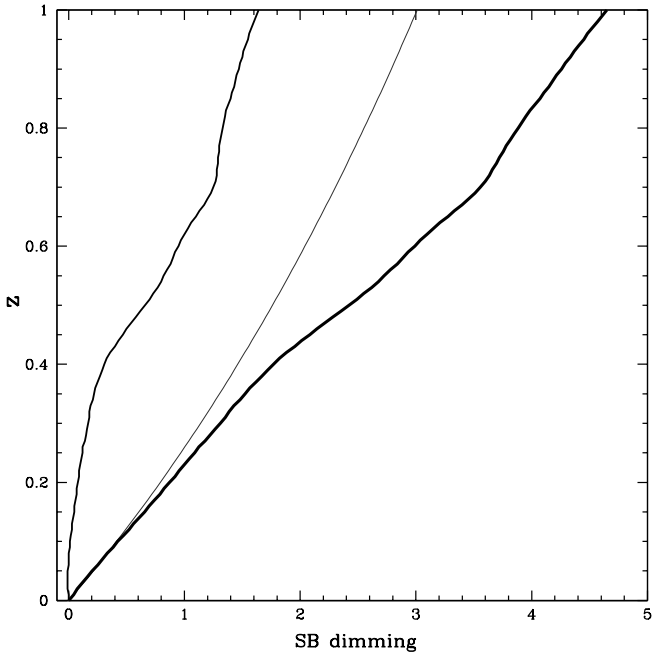

FIG. 1.—Combining the *K*-correction with surface brightness dimming, in magnitudes, as a function of redshift. The Annis *r*-band BCG *K*-correction is on the left, the thin line in the center is 10 log $(1+z)$, and the thick line on the right is the sum of the two effects.

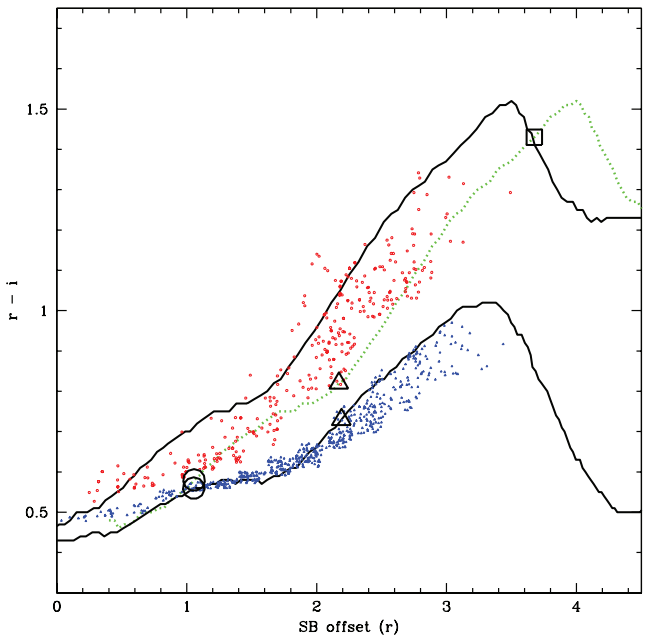

FIG. 2.—Color vs. surface brightness dimming for different galaxy types. The *x*-axis is the Annis *r*-band *K*-correction plus $(1+z)^{-4}$, and the *y*-axis is the difference between the *K*-corrected *r* band and *i* band. Redshift increases along the lines. The leftmost lines represent the BCG *K*-correction, with the right (green) one shifted by 0.5 mag with respect to the other. The rightmost line is the Sa *K*-correction. The points represent the reddest 10% (*red symbols*) and reddest 20%–30% (*blue symbols*) of galaxies in the SHELS sample. The large geometric figures point to interesting regions described in the text.

2.2. *SDSS*

From the SDSS we use the Petrosian *r* magnitudes (for a discussion of the advantages of Petrosian magnitudes for cosmological investigations, see Strauss et al. 2002), the star/galaxy classifications, and the colors derived from the fiber magnitudes. From the Petrosian half-light radii (in the *r* band) we calculate the central surface brightness μ_r, the average surface brightness (in *r* mag arcsec^{-2} inside the half-light radius):

$$\mu_r \equiv M_{\mathrm{Pet},r} + 2.5\left[0.798 + 2\log(R_{\mathrm{Pet},50,r})\right],$$

where $M_{\mathrm{Pet},r}$ is the Petrosian *r* magnitude and $R_{\mathrm{Pet},50,r}$ is the Petrosian half-light radius in the *r* band. All measures are extinction-corrected. In § 6 we calibrate the $[\mu_r, (r-i)]$ plane to redshift for the SDSS, using μ_r, $(r-i)$, and redshift.

2.3. *SHELS*

The SHELS will be a magnitude-limited redshift survey when complete. We use the data set as of 2006 January 1. Our data set is 90% complete to $R < 19.7$ and is 50% differentially complete at $R = 20.3$, using DLS total magnitudes.

From the full SHELS data set we eliminated all objects in the vicinity of bright stars (about 5%); we discarded any object where the DLS position differs from the SDSS position by more than 1″; we used only galaxies with spectra with secure redshifts. The final sample contains 8529 redshifts of the estimated final 12,000.

2.4. *The Combination*

The key data set required for the μ-PhotoZ technique is a photometrically complete sample of galaxies with accurate central surface brightnesses and at least one color. For this paper we primarily use μ_r and the $r-i$ color from the SDSS DR4. In addition, we derive a set of pseudomagnitudes: $\mu_g = \mu_r + (g-r)$, $\mu_i = \mu_r - (r-i)$, and $\mu_z = \mu_r - (r-z)$. These are estimates of the surface brightness inside the half-light radius defined by the *r* band.

3. TECHNIQUE

Surface brightness, which in an expanding universe changes as $(1+z)^{-4}$ (Tolman 1930), is a much more sensitive indicator of redshift than apparent magnitude. Unlike apparent magnitude, surface brightness has no dependence on the details of the cosmology (e.g., Sandage 1975).

The change in the observed surface brightness of a galaxy is the product of the change in brightness due to the use of a static (nonredshifted) bandpass (the *K*-correction; Hubble 1936) and cosmological dimming. Figure 1 shows these effects in terms of the measured dimming in magnitudes as a function of the redshift of the object. The line on the left is the *K*-correction for *r*-band measurements of brightest cluster galaxies calculated by J. Annis[1] using the Pegase code (Le Borgne & Rocca-Volmerange 2002). The thin line in the middle is simply 10 log $(1+z)$, and the thick line on the right is the product of the two effects.

When the galaxies in the catalog are binned according to μ_r and then sorted by color, the reddest 10%–20% of the galaxies in each μ_r bin show a very strong correlation between μ_r and redshift.

Figure 2 explains this correlation. The *y*-axis is simply the $r-i$ color. The *x*-axis represents the surface brightness dimming expected from the sum of the appropriate *K*-correction and the 10 log $(1+z)$ effect. The lines on the plot represent the $r-i$ color of galaxies computed by subtracting the Annis *K*-correction model in the *i* band from the model in the *r* band. On the left the two lines represent the BCG galaxy model (*black line*) and that model shifted 0.5 mag (*dashed green line*) to approximate the extent of the scatter. On the right, Figure 2 shows the model for an Sa galaxy

[1] See http://home.fnal.gov/~annis/astrophys/kcorr/kcorr.html.

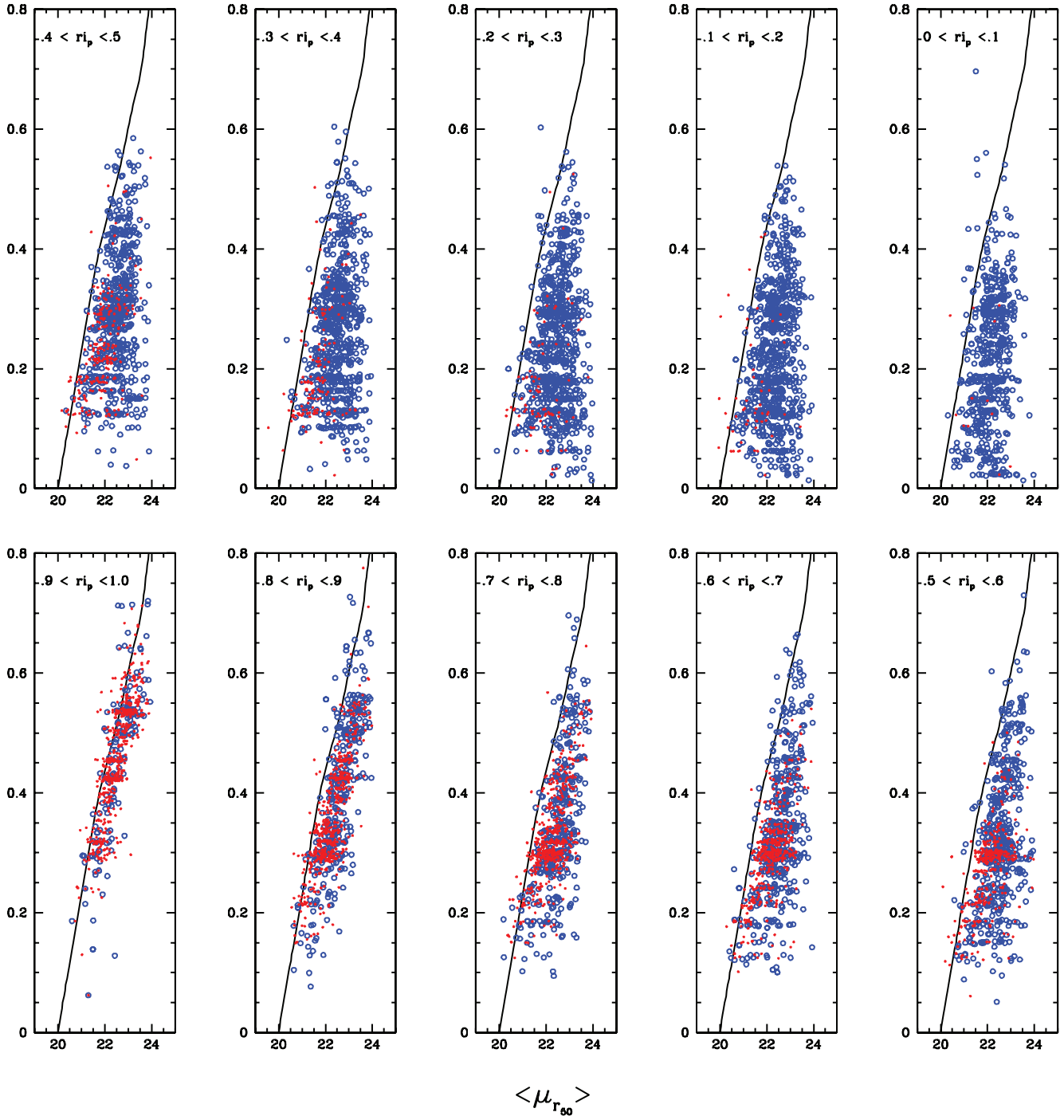

FIG. 3.—Redshift–surface brightness diagram for 10 deciles in r surface brightness sorted by $(r - i)$ color (CRP; see text). The blue circles are objects with clear O [II] emission, and the red dots are absorption-line objects.

(*black line*); we have shifted the zero point of the Sa relation by 0.46 mag to account for the difference in μ_r between a $r^{1/4}$ law galaxy and an exponential disk with the same scale length and total magnitude (Strauss et al. 2002). Redshift increases along the lines.

The small red circles show the observed $r - i$ color and $\mu_r -$ const for those galaxies in the reddest 10% in each μ_r bin which have a measured redshift, and the small blue triangles show the 20%–30% reddest objects in each bin. As expected, the redder objects lie mainly between the two BCG lines, and the bluer objects approximately follow the SA line, validating our use of these models.

A successful technique which calibrates red galaxies to redshift must be free of contamination by higher redshift blue objects at the same color. Figure 2 shows that surface brightness eliminates much of the possible confusion. There are, however, regions in Figure 2 where lines cross or come close to each other, indicating degeneracies.

There are three sets of large geometric figures in the plot: the left (lower) two sets (*circles and triangles*) show regions where there could be confusion between BCG galaxies and Sa galaxies, indicating possible problems for the technique; the right (upper) square(s), which overlap perfectly, show where BCG galaxies no

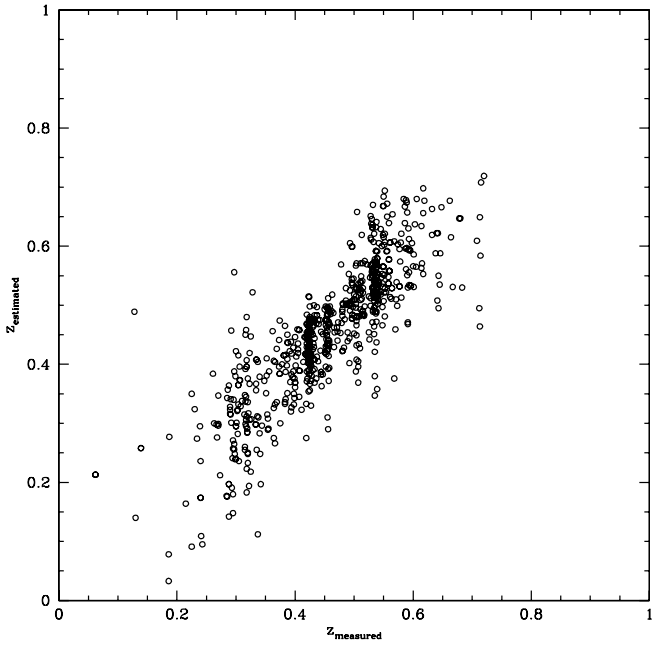

FIG. 4.—Comparison of the predicted and measured redshifts obtained by applying the model to the reddest 10% of galaxies.

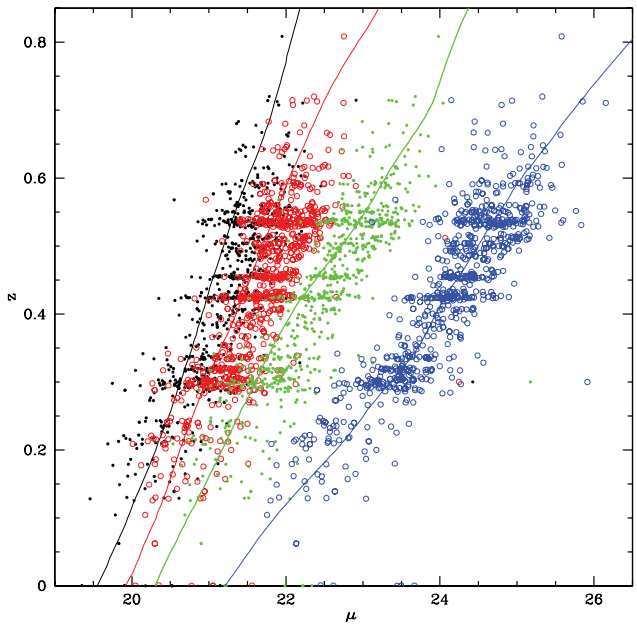

FIG. 5.—Surface brightness–redshift relation for different color bands, for the reddest 10% in $(r - i)$ selected at fixed μ_r. The leftmost black dots are the z-band measures, the red circles are i, the green dots are r, and the rightmost blue circles are g. The lines are the Annis BCG K-correction for the appropriate color.

longer become redder in $r - i$ with increasing redshift, indicating a limit to the μ-PhotoZ technique.

The circles on the bottom left show where the BCG galaxy is at $z = 0.15$ and the SA galaxy is at $z = 0.24$. Clearly, if a calibration of red objects to redshift as a function of μ_r succeeds at this redshift, it is not because it separates early-type galaxies from SA galaxies.

The pair of triangles are at $z = 0.4$ for the BCG and $z = 0.5$ for the SA. They are close enough to present a potential problem. We note that P05 found increased scatter in their calibration of photometric redshifts for large red galaxies (LRGs) at $z = 0.4$, but attributed it to other causes. Note that it is the (approximately) 0.45 mag difference between the BCG and Sa central surface brightnesses at a fixed magnitude which separates the types in the color-magnitude diagram in Figure 2; previous methods, such as that of P05, use total magnitudes and additional colors. Using surface brightness breaks this degeneracy for galaxies with different surface brightness profiles without requiring additional colors to be observed. The top square(s), at $z = 0.65$ for the unshifted BCG locus and $z = 0.765$ for the shifted locus, clearly show a region where the $10 \log (1 + z)$ dimming is insufficient to remove degeneracies.

To summarize the technique: using a complete photometric catalog (e.g., SDSS) we (1) bin galaxies according to a measure of central surface brightness, such as μ_r, then (2) in each bin, we sort the galaxies by a measure of color, such as $r - i$. Next (3) we assign a percentile rank to each galaxy based on its color, within each surface brightness bin.

As an example, in the F2 field there are 2506 galaxies with μ_r between 22.6 and 22.8; a galaxy at $\mu_r = 22.79$ and with $r - i = 0.965$ is redder than 96.2% of the galaxies in its bin and receives a color percentile of 96.2. Likewise, a galaxy with $\mu_r = 22.38$ and with $r - i = 0.769$ is redder than 96.2% of the 1551 galaxies in the $\mu_r = 22.2$–22.4 mag bin. Note that both galaxies have a color rank score of 96.2 but have substantially different actual $r - i$ colors.

These color rank percentile (CRP) scores are strongly correlated with galaxy type. In the next section we demonstrate their usefulness in permitting a calibration of central surface brightness to redshift for the redder objects.

3.1. *Results*

Figure 3 shows the result of plotting μ_r versus redshift for galaxies within 10 decile bins in CRP scores. We compute ranks using the $r - i$ color. The red dots are for spectra where the measured O [II] λ3727 equivalent width is greater than -2 Å, and the blue circles have clearly measurable emission ($EW_{3727} < -2$ Å). The solid lines are the Annis r-band BCG K-correction times $10 \log (1 + z)$ shifted to match $\mu_r = 20.0$ mag arcsec^{-2} at redshift zero.

There are several things to notice in Figure 3. First the galaxies in the reddest deciles in CRP follow the prediction of the Annis BCG K-correction times $10 \log (1 + z)$ very closely. The next decile is slightly offset from the reddest. Clearly, the calibration of μ_r to redshift for galaxies in these CRP deciles is straightforward.

Next we notice that the bluest objects show essentially no correlation between μ_r and redshift; the available μ_r-z space in the bluest decile in CRP is nearly uniformly filled. Clearly, μ_r cannot be calibrated to redshift for the bluest objects, which have their surface brightnesses altered by star formation.

Figure 4 shows the result of fitting μ_r to redshift by finding the redshift z for which

$$\mu_r(i) = K_i(z) + 10 \log (1 + z) + 19.45 + 3.3[1 - \mathrm{CRP}(i)]$$

for the ith galaxy (the model). The factor containing CRP accounts for the change in μ_r with color, variously quantified as the color-magnitude relation for elliptical galaxies (e.g., Baum 1959; Visvanathan & Sandage 1977; Chang et al. 2006; Cool et al. 2006; Eisenhardt et al. 2007) or as the fundamental plane (e.g., Djorgovski & Davis 1987; Bernardi et al. 2003).

The standard deviation for the entire sample of the reddest 10% in Figure 4 is $\sigma(\Delta z/1 + z) = 0.046$ and is $\sigma = 0.056$ for the reddest 10%–20%. This result is comparable with the best current

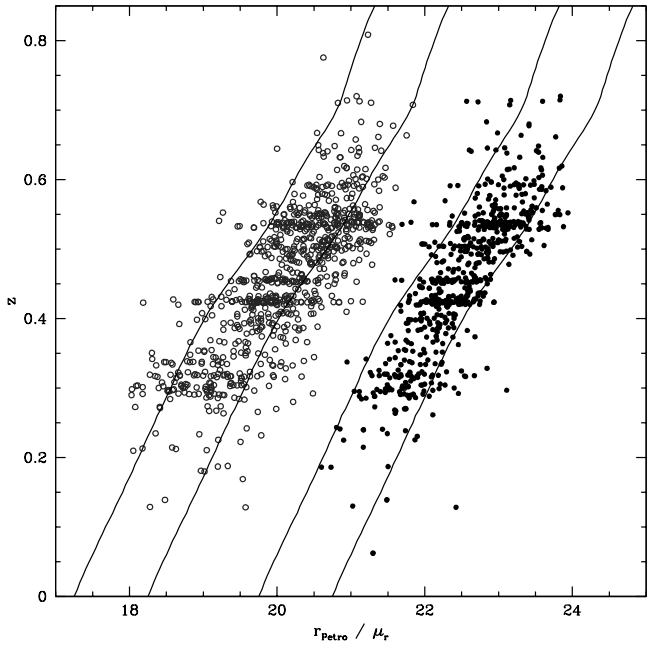

FIG. 6.—Difference between the reddest 10% using total Petrosian magnitudes (*left lines*) and μ_r (*right lines*). Note the decreased scatter for μ_r.

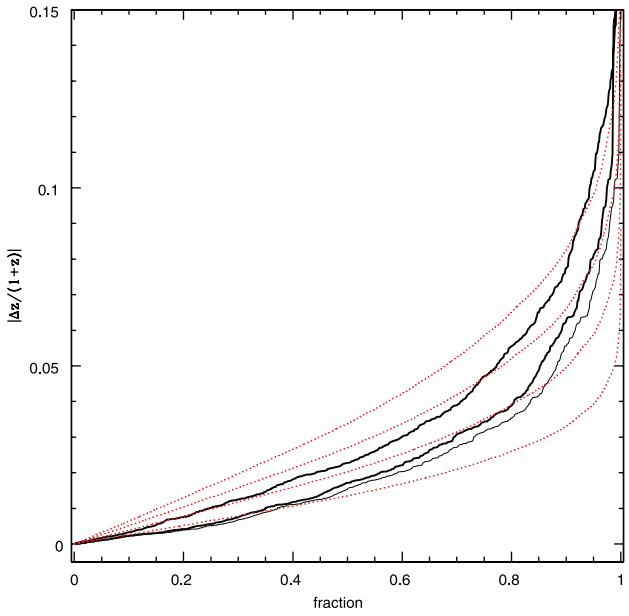

FIG. 7.—Sorted absolute value of the errors of the technique in § 5. The red dotted lines represent normal error distributions, with σ values of 0.05 (*top line*), 0.04, 0.03, and 0.02 (*bottom line*). The thick lines represent the actual data for the reddest 80%–90% (*upper thick line*) and the reddest 90%–100% (*lower thick line*). The thin solid line and the lower solid thick line differ by the removal of all objects with $(g - r) < 1.4$ for the thin line.

photometric redshifts for the LRGs. P05 obtain $\sigma = 0.035$ using g photometry, as well as r and i (see § 5).

4. USING OTHER COLORS AND MAGNITUDES

As Figure 2 shows, the μ-PhotoZ technique becomes degenerate when the 4000 Å break enters the bandpass of the reddest band (i in Fig. 2). To acquire μ-PhotoZ values for higher redshift objects, observations in a redder passband (z, J, H, etc.) would extend the technique to higher redshifts. Neither the SHELS spectroscopy nor the SDSS photometry go deep enough to test the technique for redshifts greater than 0.65 using z-band photometry.

Obviously, other bandpasses may also be used. There are three different choices to make: (1) the bandpass to use to sort the colors, (2) the color to use, and (3) the bandpass to fit. Here we have used μ_r, $(r - i)$, and μ_r, but other choices are informative. Figure 5 shows galaxies in the reddest 10% as determined using μ_r and $(r - i)$ versus μ_z, μ_i, μ_r, and μ_g, along with the sum of 10 log $(1 + z)$ and the appropriate Annis BCG K-correction for each color. Redshift estimates using z- and g-band data have larger errors than estimates using r and i, in the manner expected from the larger published errors in the SDSS magnitudes for these bands.

One might also ask whether the technique of using color ranks might also work if one uses total magnitude rather than central surface brightness. Figure 6 (*left curves*) shows galaxies in the reddest 10% in $(r - i)$ measured at fixed Petrosian r magnitude versus Petrosian r, and (*right curves*) galaxies in the reddest 10% in $(r - i)$ measured at fixed μ_r versus μ_r; each grouping has two lines to guide the eye. These lines are the product of the K-correction and the surface brightness dimming. The separation is an arbitrary 1 mag.

Clearly, the scatter in the Petrosian magnitude measures in Figure 6 is larger than in the μ_r measures. Figure 2 explains this behavior. Recall that we shifted the line representing the K-correction and surface brightness dimming by 0.46 mag to account for a 0.46 difference in the mean central surface brightness at fixed total magnitude for the two galaxy types (BCG and Sa), and this procedure matched the data. Shifting the Sa line 0.46 mag brightward would place it much closer to the BCG line, and would thus produce substantially more degeneracy in the color rank approach.

5. CALIBRATING THE RELATION DIRECTLY

In § 3.1 we demonstrated that we can predict the redshift of a red galaxy accurately from a measure of its central surface brightness and a single color $(r - i)$. We fitted models based on estimates of the K-correction, the color-magnitude relation for elliptical galaxies, and the $(1 + z)^{-4}$ cosmological dimming to measures of color and surface brightness.

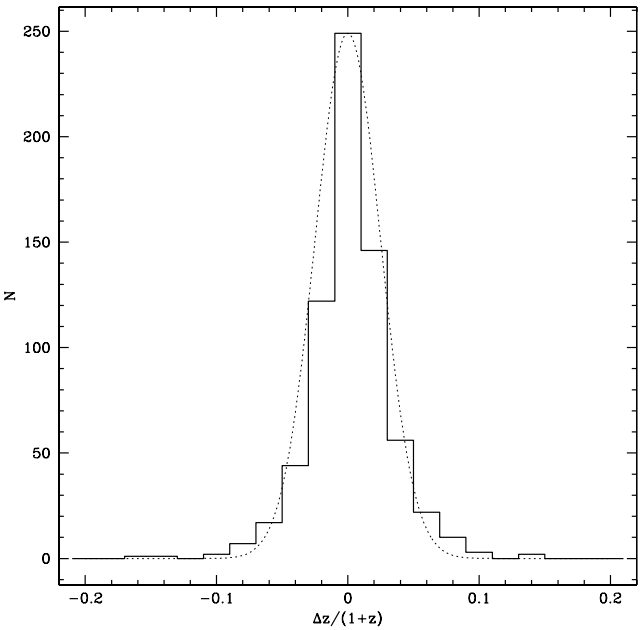

FIG. 8.—Error distribution $[\Delta z/(1 + z)]$ for the 80%–100% reddest objects, with the $(g - r) < 1.4$ objects removed. The Gaussian has $\sigma = 0.025$.

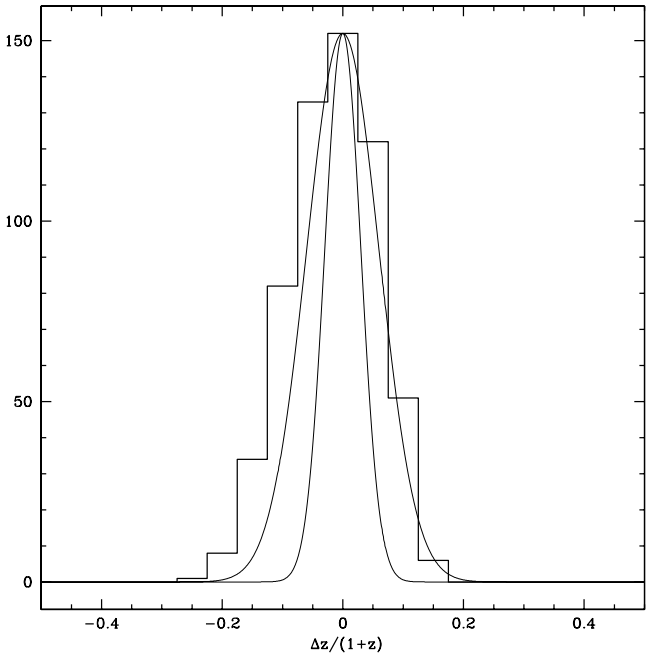

FIG. 9.—Error distribution $[\Delta z/(1+z)]$ for the 80%–100% reddest objects, with $(g-r) < 1.4$. Gaussians with $\sigma = 0.030$ and $\sigma = 0.06$ are superposed. Note the change in scale from Fig. 8.

We may not have used the best model parameters in making these fits, and we can also suspect that our measure of central surface brightness μ_r could have measurement systematics which correlate with redshift. Although these models are useful in understanding the physical basis for the technique, they are not actually required to implement it.

Rather than attempt to optimize the models and measures, we choose to calibrate the data directly. To each galaxy we assign the median redshift of its neighbors in μ_r-CRP space, excluding the galaxy itself, in jackknife fashion.

Figure 7 shows the distribution of absolute values of the residuals [in terms of $\Delta z/(1+z)$]; the thick black lines represent the residuals of the actual data (the upper thick line represents galaxies in the 80%–90% color range, and the lower represents those in the 90%–100% color range), sorted from smallest to largest. The dotted lines show the distributions expected for normal error distributions with σ values of (*bottom to top*) 0.02, 0.03, 0.04, and 0.05. The tails of the error distribution are clearly not Gaussian, but the errors are small. Eighty percent of all objects in the reddest decile have errors smaller than would be expected for a normal error distribution with a σ of 0.03.

About 40% of the high-residual objects are low-redshift galaxies that are anomalously blue in $g-r$. These objects could easily be removed in a three-band survey. For example, the thin solid line in Figure 7 shows the error distribution for the same sample as the bottom solid line, but with all objects with $g-r < 1.4$ removed. The tails of the distribution are substantially reduced.

TABLE 1

REDSHIFT VS. μ_r AND $(r-i)$

μ_r	0.50	0.55	0.60	0.65	0.70	0.75	0.80	0.85	0.90	0.95	1.00	1.05	1.10	1.15	1.20
20.40.....															
20.50.....															
20.60.....	0.228[a]	0.258[a]													
20.70.....	0.246[b]	0.255[c]													
20.80.....	0.235[b]	0.265[b]													
20.90.....	0.247[b]	0.262[b]	0.289[c]	0.336[a]											
21.00.....	0.247[b]	0.268[b]	0.297[d]	0.287[a]											
21.10.....	0.252[b]	0.275[b]	0.295[c]	0.316[c]											
21.20.....	0.258[b]	0.280[c]	0.307[c]	0.312[d]	0.294[a]										
21.30.....	0.262[c]	0.282[c]	0.314[c]	0.329[c]	0.331[a]										
21.40.....	0.266[c]	0.292[c]	0.318[c]	0.335[c]	0.366[c]										
21.50.....	0.271[c]	0.296[c]	0.322[c]	0.345[c]	0.353[d]										
21.60.....	0.280[c]	0.303[c]	0.327[c]	0.343[c]	0.366[c]	0.391[d]									
21.70.....	0.295[c]	0.313[c]	0.335[c]	0.353[c]	0.370[c]	0.400[d]									
21.80.....	0.303[c]	0.319[c]	0.337[c]	0.353[c]	0.375[c]	0.409[d]	0.422[d]	0.421[d]							
21.90.....	0.305[c]	0.320[c]	0.342[c]	0.361[c]	0.382[c]	0.414[c]	0.432[c]	0.458[d]							
22.00.....	0.318[c]	0.330[c]	0.343[c]	0.364[c]	0.388[c]	0.409[c]	0.432[c]	0.450[c]	0.469[a]	0.476[a]					
22.10.....	0.319[c]	0.334[c]	0.351[c]	0.371[c]	0.396[c]	0.419[c]	0.440[c]	0.455[c]		0.466[a]					
22.20.....	0.327[c]	0.341[c]	0.357[c]	0.377[c]	0.398[c]	0.421[b]	0.444[c]	0.458[c]	0.466[b]	0.471[a]	0.479[a]				
22.30.....	0.337[c]	0.346[c]	0.363[c]	0.382[c]	0.404[c]	0.425[c]	0.439[b]	0.452[c]	0.471[b]	0.475[c]	0.488[a]				
22.40.....	0.343[c]	0.354[c]	0.365[c]	0.388[c]	0.403[c]	0.427[b]	0.444[b]	0.463[c]	0.471[b]	0.480[d]	0.478[a]				
22.50.....	0.352[c]	0.361[c]	0.374[c]	0.391[c]	0.410[c]	0.429[c]	0.448[b]	0.458[b]	0.473[c]	0.485[b]	0.490[d]	0.505[a]			
22.60.....	0.360[c]	0.367[c]	0.382[c]	0.395[c]	0.416[c]	0.435[b]	0.450[b]	0.463[b]	0.476[c]	0.489[d]	0.496[d]				
22.70.....	0.364[c]	0.363[d]	0.381[c]	0.402[c]	0.420[c]	0.441[b]	0.456[b]	0.466[b]	0.472[b]	0.489[b]	0.500[b]	0.509[d]	0.509[c]		
22.80.....	0.380[d]	0.373[c]	0.393[c]	0.410[c]	0.421[c]	0.445[b]	0.460[c]	0.468[b]	0.481[b]	0.485[d]	0.503[c]		0.523[a]		
22.90.....	0.358[d]	0.386[c]	0.403[c]	0.415[c]	0.429[c]	0.451[c]	0.455[b]	0.472[b]	0.483[b]	0.494[b]	0.504[c]	0.514[b]	0.524[a]	0.535[a]	
23.00.....	0.397[c]	0.388[d]	0.405[d]	0.419[c]	0.439[c]	0.451[c]	0.464[b]	0.478[b]	0.484[b]		0.505[b]	0.523[b]	0.548[a]		
23.10.....	0.401[d]	0.398[c]	0.413[c]	0.429[c]	0.445[c]	0.458[c]	0.468[b]	0.483[b]	0.484[d]	0.502[b]	0.512[d]	0.528[a]		0.515[a]	
23.20.....		0.405[c]	0.424[c]	0.429[d]	0.449[c]	0.463[c]	0.474[d]	0.488[d]	0.489[b]	0.509[b]	0.500[a]		0.537[a]	0.539[a]	

NOTES.—The letters indicate the measured errors in each cell, where σ_1 is the estimate of $\sigma_{\Delta z/(1+z)}$ obtained at the 68% point in the error distribution and σ_2 is obtained at the 95% point. (a) $\sigma_1 < 0.035$, σ_2 undefined (fewer than 30 objects in the bin); (b) $\sigma_1 < 0.025$, $\sigma_2 < 0.035$; (c) $\sigma_1 < 0.035$, $\sigma_2 < 0.05$; (d) $\sigma_1 < 0.05$, $\sigma_2 < 0.07$.

Figure 8 shows the distribution of residuals for the reddest 20% (excluding $g - r < 1.4$) of $(z_{\rm meas} - z_{\rm est})/(1 + z)$ with a $\sigma = 0.025$ Gaussian overplotted (1272 objects with redshifts). These results show that μ-PhotoZ redshifts are as accurate as the best photometric redshifts, (e.g., P05). The 1 σ rms for the data in Figure 8 is 0.030; P05 obtain 0.035. The (μ_r, CRP)-z calibration works well for all galaxies with $(g - r) > 1.4$. The 1 σ rms for all these 2399 galaxies with redshifts is 0.037.

Figure 7 clearly indicates that the μ-PhotoZ method provides estimated redshifts from a single color, such as $r - i$, albeit with increased errors and a non-Gaussian error component. Figure 9 shows the error distribution $\Delta z/(1 + z)$ for the 330 galaxies from SHELS which are in the reddest 20% and which have $g - r <$ 1.4; two Gaussians, with $\sigma = 0.03$ and 0.06, are also plotted.

The error distribution in Figure 9 for $\Delta z/(1 + z)$ can be reasonably fitted by a Gaussian with $\sigma = 0.06$ and a non-Gaussian tail, where the actual redshifts are always smaller than the estimated ones. A description of the tail, consistent with the current data, is that the objects are randomly located in the galaxy distribution in the foreground of its apparent (as estimated by μ-PhotoZ) position, $z_{\rm est}$.

For the entire sample of the 20% reddest galaxies, without removing any objects using a third band, the error distribution for $z_{\rm est}$ is

$$\mathrm{Err}_{z_{\rm est}} = 0.79G(0.03) + 0.16G(0.06) + 0.05R(N(z)), \quad z < z_{\rm est},$$

where $G(x)$ is a Gaussian with $\sigma = x$, $R(x)$ is a random deviate from the distribution x, and $N(z)$ is the redshift distribution of the "foreground" galaxies.

6. CALIBRATING THE SDSS μ_r, $(r - i)$ TO REDSHIFT RELATION FOR RED GALAXIES

The color percentile measure at any fixed surface brightness corresponds directly to an actual color. To provide a calibration for the SDSS we simply find the median redshift for galaxies in small cells in μ_r, $(r - i)$.

We use the SDSS DR5 and find the 62,259 galaxies with $20.35 < \mu_r < 23.25$ and $0.475 < (r - i) < 1.225$ and with $(g - r) > 1.4$ which have measured redshifts. There are 59,905 redshifts from the SDSS, essentially the LRG sample (Eisenstein et al. 2001), and 2345 redshifts come from SHELS, mainly for fainter galaxies. There are 64 objects in common. The redshifts agree, save for one case where SDSS found a star and SHELS found a galaxy.

To estimate the error in the redshift estimator we take, for each cell, the galaxies in the cell and assign to them the median redshift for that cell. We then rank the absolute value of the residuals for the galaxies in that cell. The median residual for a Gaussian distribution would be 0.67 σ, the 68th percentile would be 1 σ, and the 95th percentile would be 2 σ. We only estimate the 1 σ point if there are at least 15 galaxies in a bin, and the 2 σ point if there are more than 30.

Table 1 displays the results for bins with small and well-determined residuals in a convenient form. The footnotes indicate the error. Use of this table allows quick and reasonably accurate estimation of redshifts for red galaxies in the SDSS photometric database, reaching to a redshift of approximately 0.5.

7. DISCUSSION

Surface brightness is a fundamental observational parameter of galaxies; it is directly related to redshift through the classical Tolman effect. We believe this investigation is the first to show in detail that surface brightness may be used directly as a measure of redshift, the μ-PhotoZ method.

We demonstrate the value of surface brightness measures in determining photometric redshifts using three different techniques. First we use a model which emphasizes the physical and measurement aspects of the problem. Next we demonstrate that by assigning a galaxy the median redshift of its neighbors in surface brightness–color percentile space, we can achieve photometric redshift errors comparable with the best current photometric redshift methods. Finally, by taking the median redshift in small bins in surface brightness–color space we develop a redshift estimator with errors comparable with the best techniques.

Although we have concentrated on the use of μ_r and $(r - i)$ for nearby red galaxies, the techniques discussed here have much greater generality; the $(1 + z)^{-4}$ cosmological dimming affects all galaxies at all redshifts. Adding surface brightness directly into model fitting and hybrid methods seems a very profitable avenue to explore.

Obviously, the technique could be extended to greater redshift for red galaxies by using the z band. Deep, large-area lensing surveys, including the DLS, often have deep z photometry, and thus can obtain photometric redshifts out to a redshift of about 1 using the methods shown here. These deeper surveys will also be able to eliminate some of the non-Gaussian error apparent in the SDSS photometry. Much of this error results from SDSS failure to separate close pairs of faint objects (star+galaxy or galaxy+galaxy). With much deeper imaging and better seeing these effects should be less troublesome.

As the discussion in § 5 makes clear, most of the benefit from applying the μ-PhotoZ technique is achieved by using just two photometric bands. This powerful aspect of the technique has obvious implications for the design of large-area weak-lensing surveys. It is exactly the high central surface brightness red galaxies analyzed in § 5 which have the highest redshift at fixed central surface brightness (Fig. 3), and central surface brightness is the limiting factor in determining the shape parameters for the sources. Our technique makes feasible substantially larger area weak-lensing surveys than would be possible were it necessary to observe through several filters.

We thank Scott Kenyon for discussions, and we thank Tony Tyson, David Wittman, and Vera Margoniner for their collaboration in obtaining the initial galaxy catalog. We thank Ken Rines and Warren Brown for a careful reading of the manuscript. This research was supported in part by the Smithsonian Institution.

REFERENCES

Adelman-McCarthy, J. K., et al. 2006, ApJS, 162, 38
Baum, W. A. 1957, AJ, 62, 6
———. 1959, PASP, 71, 106
———. 1962, in IAU Symp. 15, Problems of Extra-Galactic Research, ed. G. C. McVittie (New York: MacMillan), 390
Bernardi, M., et al. 2003, AJ, 125, 1866
Bolzonella, M., Miralles, J.-M., & Pelló, R. 2000, A&A, 363, 476
Budavári, T., et al. 2001, AJ, 122, 1163
Chang, R., Shen, S., Hou, J., Shu, C., & Shao, Z. 2006, MNRAS, 372, 199
Cool, R. J., Eisenstein, D. J., Johnston, D., Scranton, R., Brinkmann, J., Schneider, D. P., & Zehavi, I. 2006, AJ, 131, 736
Djorgovski, S., & Davis, M. 1987, ApJ, 313, 59
Eisenhardt, P. R., De Propris, R., Gonzalez, A., Stanford, S. A., Dickinson, M. E., & Wang, M. C. 2007, ApJS, 169, 225
Eisenstein, D. J., et al. 2001, AJ, 122, 2267
Fabricant, D., et al. 2005, PASP, 117, 1411

Feldmann, R., et al. 2006, MNRAS, 372, 565
Firth, A. E., Lahav, O., & Somerville, R. S. 2003, MNRAS, 339, 1195
Geller, M. J., Dell'Antonio, I. P., Kurtz, M. J., Ramella, M., Fabricant, D. G., Caldwell, N., Tyson, J. A., & Wittman, D. 2005, ApJ, 635, L125
Hubble, E. 1936, ApJ, 84, 517
Hubble, E., & Tolman, R. C. 1935, ApJ, 82, 302
Kodama, T., Bell, E. F., & Bower, R. G. 1999, MNRAS, 302, 152
Le Borgne, D., & Rocca-Volmerange, B. 2002, A&A, 386, 446
Margoniner, V. E., Connolly, A., & Tyson, J. A. 2005, BAAS, 37, 1206
Margoniner, V. E., & Wittman, D. M. 2007, ApJ, submitted (arXiv: 0707.2403)
Padmanabhan, N., et al. 2005, MNRAS, 359, 237 (P05)
Pahre, M. A., Djorgovski, S. G., & de Carvalho, R. R. 1996, ApJ, 456, L79
Sandage, A. 1975, in Galaxies and the Universe, ed. A. Sandage, M. Sandage, & J. Kristian (Chicago: Univ. Chicago Press), 761
Sandage, A., & Lubin, L. M. 2001, AJ, 121, 2271
Strauss, M. A., et al. 2002, AJ, 124, 1810
Suchkov, A. A., Hanisch, R. J., & Margon, B. 2005, AJ, 130, 2439
Tolman, R. C. 1930, Proc. Natl. Acad. Sci., 16, 511
Visvanathan, N., & Sandage, A. 1977, ApJ, 216, 214
Wadadekar, Y. 2005, PASP, 117, 79
Wittman, D., Dell'Antonio, I. P., Hughes, J. P., Margoniner, V. E., Tyson, J. A., Cohen, J. G., & Norman, D. 2006, ApJ, 643, 128